

Plasmon-induced transparency effect in hybrid terahertz metamaterials with active control and multi-dark modes

Yuting Zhang(张玉婷), Songyi Liu(刘嵩义), Wei Huang(黄巍), Erxiang Dong(董尔翔), Hongyang Li(李洪阳), Xintong Shi(石欣桐), Meng Liu(刘蒙), Wentao Zhang(张文涛), Shan Yin(银珊), and Zhongyue Luo(罗中岳)

Citation: Chin. Phys. B, 2022, 31 (**6**): 068702. DOI: 10.1088/1674-1056/ac4f56
Journal homepage: http://cpb.iphy.ac.cn; http://iopscience.iop.org/cpb

What follows is a list of articles you may be interested in

Terahertz generation and detection of LT-GaAs thin film photoconductive antennas excited by lasers of different wavelengths

Xin Liu(刘欣), Qing-Hao Meng(孟庆昊), Jing Ding(丁晶), Zhi-Chen Bai(白志晨), Jia-Hui Wang(王佳慧), Cong Zhang(张聪), Bo Su(苏波), and Cun-Lin Zhang(张存林)

Chin. Phys. B, 2022, 31 (**2**): 028701. DOI: 10.1088/1674-1056/ac0cd5

Optical strong coupling in hybrid metal-graphene metamaterial for terahertz sensing

Ling Xu(徐玲), Yun Shen(沈云), Liangliang Gu(顾亮亮), Yin Li(李寅), Xiaohua Deng(邓晓华), Zhifu Wei(魏之傅), Jianwei Xu(徐建伟), and Juncheng Cao(曹俊诚)

Chin. Phys. B, 2021, 30 (**11**): 118702. DOI: 10.1088/1674-1056/abfb58

Terahertz polarization conversion and sensing with double-layer chiral metasurface

Zi-Yang Zhang(张子扬), Fei Fan(范飞), Teng-Fei Li(李腾飞), Yun-Yun Ji(冀允允), Sheng-Jiang Chang(常胜江)

Chin. Phys. B, 2020, 29 (**7**): 078707. DOI: 10.1088/1674-1056/ab9294

Applications of nanostructures in wide-field, label-free super resolution microscopy

Xiaowei Liu(刘小威), Chao Meng(孟超), Xuechu Xu(徐雪初), Mingwei Tang(汤明炜), Chenlei Pang(庞陈雷), Qing Yang(杨青)

Chin. Phys. B, 2018, 27 (**11**): 118704. DOI: 10.1088/1674-1056/27/11/118704

Transient optical modulation properties in the terahertz metamaterial of split ring resonators

Zhou Qing-Li,Shi Yu-Lei,Wang Ai-Hua,Li Lei,Zhang Cun-Lin

Chin. Phys. B, 2012, 21 (**5**): 058701. DOI: 10.1088/1674-1056/21/5/058701

Plasmon-induced transparency effect in hybrid terahertz metamaterials with active control and multi-dark modes

Yuting Zhang(张玉婷)[1], Songyi Liu(刘嵩义)[1], Wei Huang(黄巍)[1,†], Erxiang Dong(董尔翔)[1], Hongyang Li(李洪阳)[1], Xintong Shi(石欣桐)[1], Meng Liu(刘蒙)[2], Wentao Zhang(张文涛)[1], Shan Yin(银珊)[1], and Zhongyue Luo(罗中岳)[1]

[1] *Guangxi Key Laboratory of Optoelectronic Information Processing, School of Optoelectronic Engineering, Guilin University of Electronic Technology, Guilin* 541004, *China*

[2] *College of Electronic and Information Engineering, Shandong University of Science and Technology, Qingdao* 266590, *China*

(Received 17 December 2021; revised manuscript received 17 January 2022; accepted manuscript online 27 January 2022)

We numerically demonstrate a photo-excited plasmon-induced transparency (PIT) effect in hybrid terahertz (THz) metamaterials. The proposed metamaterials are regular arrays of hybrid unit cells composed of a metallic cut wire and four metallic split-ring resonators (SRRs) whose gaps are filled with photosensitive semiconductor gallium arsenide (GaAs) patches. We simulate the PIT effect controlled by external infrared light intensity to change the conductivity of GaAs. In the absence of photo excitation, the conductivity of GaAs is 0, thus the SRR gaps are disconnected, and the PIT effect is not observed since the dark resonator (supported by the hybrid SRRs) cannot be stimulated. When the conductivity of GaAs is increased via photo excitation, the conductivity of GaAs can increase rapidly from 0 S/m to 1×10^6 S/m and GaAs can connect the metal aluminum SRR gaps, and the dark resonator is excited through coupling with the bright resonator (supported by the cut wire), which leads to the PIT effect. Therefore, the PIT effect can be dynamically tuned between the on and off states by controlling the intensity of the external infrared light. We also discuss couplings between one bright mode (CW) and several dark modes (SRRs) with different sizes. The interference analytically described by the coupled Lorentz oscillator model elucidates the coupling mechanism between one bright mode and two dark modes. The phenomenon can be considered the result of linear superposition of the coupling between the bright mode and each dark mode. The proposed metamaterials are promising for application in the fields of THz communications, optical storage, optical display, and imaging.

Keywords: metamaterial, plasmon induced transparency, photo-excited, terahertz

PACS: 87.50.U–, 78.67.Pt **DOI:** 10.1088/1674-1056/ac4f56

1. Introduction

In the electromagnetic spectrum, THz waves are located in the transition region between microwave and infrared, with a frequency range from 0.1 THz to 10 THz.[1–4] Terahertz modulators based on traditional materials are usually thick and heavy, which is not conducive to the integrated development of optical systems. Recently, using structured materials to manipulate THz waves has drawn a great deal of attention. Metamaterials, which are usually composed of artificial subwavelength periodic resonators, provide an effective means to manipulate THz waves, and they also exhibit novel electromagnetic properties which are unavailable in natural materials. Furthermore, real-time THz metamaterials can be realized by integrating functional media (such as semiconductors or phase transition materials) into metallic or dielectric metamaterials. The electromagnetic response of hybrid metamaterials can be actively modified by external excitation with an electric field or laser pulse.

Electromagnetic induced transparency (EIT) is a quantum coherent effect which occurs in a three-level atomic system. EIT media exhibit three energy level states,[5] namely a ground state $|1\rangle$, an excited state $|3\rangle$, and a metastable state $|2\rangle$. Most recently, there are few papers mentioned the relationship between quantum three-states system and THz device.[6–10] The particles absorb energy and jump directly from $|1\rangle$ to $|3\rangle$ when the EIT materials are illuminated by a probe laser, leading to a broad absorption valley in the transmission spectra. Furthermore, when a coupling laser is introduced to the above experimental system, the particles absorb energy and a jump from $|1\rangle$ to $|3\rangle$ can be realized by the following two routes: $|1\rangle \rightarrow |3\rangle$ or $|1\rangle \rightarrow |3\rangle \rightarrow |2\rangle \rightarrow |3\rangle$. Interference between the two jump routes ($|1\rangle \rightarrow |3\rangle$ or $|1\rangle \rightarrow |3\rangle \rightarrow |2\rangle \rightarrow |3\rangle$) leads to a cancellation effect on state $|3\rangle$, accompanied by an enhanced transparency window within the broad absorption valley.[11–13,15–17] EIT materials have been widely used as narrowband filters, optical storage devices, optical buffer devices, and optical switching devices.

However, realization of the conventional EIT effect in an atomic system requires a stable laser and low operating temperature, which hinders the development of research and practical application to some extent. The plasmon-induced transparency (PIT) effect occurs in the classical electromagnetic metamaterial system. The bright mode resonator can be directly excited by the incident wave, leading to a broad valley in the transmission spectrum; while the dark mode resonator is excited by near-field coupling with the bright mode res-

†Corresponding author. E-mail: weihuang@guet.edu.cn

© 2022 Chinese Physical Society and IOP Publishing Ltd

onator. The cross-coupling between the bright and dark mode resonator leads to a cancellation effect on the bright mode resonator, accompanied by an enhanced transparency window within the broad absorption valley. Recently, the analogy between the PIT effect in the metamaterials system and the EIT effect in the atomic system has drawn increasing attention, and a series of representative research results have been reported in THz and optical regimes.[18,19,21,22] Recently, Liu *et al.*[23] realized active EIT metamaterials in the THz region by employing three resonators. Surface current oscillation and magnetic field distribution were extracted to explain the physical mechanism of the PIT effect. Also, Li *et al.*[24] demonstrated that they were able to tailor the EIT effect in the THz frequency by changing the geometric parameters of the metamaterials' micro-structures. However, the electromagnetic properties of metallic and dielectric metamaterials were fixed as soon as they were fabricated; thus the versatility of metallic and dielectric metamaterials is limited.

The resonant mode and frequency of a metamaterial's micro-structure play a critical role in coupling between the bright and dark modes. Photo-excitation can modify the carriers concentration in terms of resonant mode and frequency in hybrid metamaterials. Therefore, coupling between resonators fabricated from metamaterials can be actively controlled by photo illumination.[18–20] Previous research on the PIT phenomenon mainly focused on passive modulation of metamaterials, which tailored the PIT effect by changing the geometric parameters of the micro-structure. Recently, a novel method was proposed to realize active control of the PIT effect[27] using hybrid metamaterials integrated with semiconductors. Due to excitement of photo-induced carriers by an infrared laser,[23] the conductivity of a semiconductor can reach the order of magnitude of the conductivity of a conductor.[26] In this way, the electromagnetic resonance of the proposed metamaterials can be modified in the same structure without remanufacturing.

In this paper, we proposed a novel metamaterial composed of metal and photosensitive GaAs semiconductor microstructures, to realize a photo-induced PIT effect between the non-transmission and high-transmission states. GaAs structures are inserted into the gaps of metallic split-ring resonators (SRRs) and deposited on a sapphire substrate to construct a hybrid metamaterial.

2. Structure design

The unit cell of the proposed PIT metamaterial is shown in Fig. 1. The symmetrical structure consists of an aluminum cut wire (CW) and two pairs of aluminum split-ring resonators (SRRs) whose gaps are filled with photosensitive semiconductor GaAs patches. The terahertz beam is normally incident on the metamaterial array, with polarization parallel to the CW, *i.e.*, the incident electric field E is along the y axis. The metamaterial structure is placed on a sapphire substrate. The cut wire is used as the bright mode and can be directly coupled to the incident field. The two pairs of split-ring resonators are symmetrically placed around the metal cut wire, and the four rings are each embedded in a piece of photosensitive semiconductor GaAs. The metallic resonators were made from 200-nm-thick aluminum and GaAs, fabricated in a square lattice on a 0.64-mm-thick sapphire substrate, as shown in Fig. 1(b). However, when the incidence of terahertz wave with the frequency rate of 0.1–10 THz, the GaAs semi-conductor will not induce the photoelectric effect, so we need to add additional infrared light source to achieve the photosensitive tunable performance.[29]

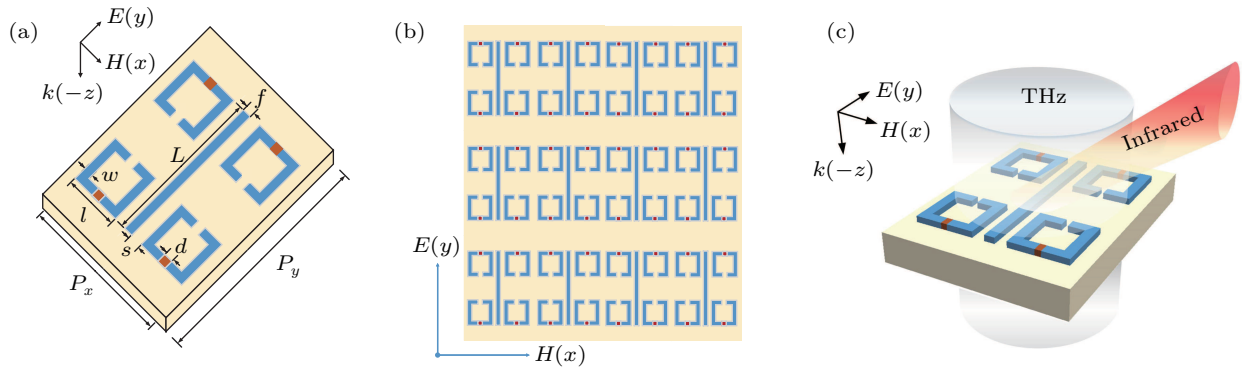


Fig. 1. (a) Schematic of a PIT metamaterials unit cell. The geometrical parameters are $L = 90$ μm, $l = 29$ μm, $w = 5$ μm, $s = 6$ μm, $d = 3$ μm, $f = 5$ μm, $P_x = 90$ μm, and $P_y = 120$ μm. (b) Top view diagram of the proposed structure array. The incident electric field is along the y direction. (c) Incidence of electromagnetic waves.

3. Active control

Using CST Microwave Studio™, we were able to further support the tunable spectral response by full-wave numerical simulation and obtain the corresponding transmission spectrum. The semiconductor material turned to metal when conductivity became very large and nearly reached the conductivity of the metal when the unit was illuminated. According to paper,[28] the conductivity of GaAs is positively correlated with light intensity. Without the addition of the infrared field and the thermal radiation, the conductivity of

GaAs can be considered to be $\sigma = 0$ S/m, with little effect on the results. In order to make the valence band electrons of GaAs with absorbing photon energy, transition to the conduction band and form hole–electron pairs, so that the conductivity of GaAs is greatly improved and gradually "metallized", the wavelength of incident light should meet the following requirements: $\lambda \leq 1240/E_g$, where E_g is the bandgap width and the value is 1.4 eV. According to the equation, it can be concluded that the wavelength of the excitation light is less than or equal to 885 nm, and corresponding the frequency is greater than 338 THz. The infrared frequency is much larger than 1 THz in the simulation. When the incidence of terahertz wave with frequency 0.1 THz–10 THz does not induce the photoelectric effect of GaAs semiconductor. Furthermore, the infrared wave can slightly increase the conductivity of aluminum based on this theory. However, the conductivity of aluminum is large enough. Thus, infrared wave does not affect aluminum in our simulations. It is concluded that the resonance caused by infrared light does not interact with terahertz incident waves.[29,30] When the infrared light intensity reaches 60 μJ/cm^2, the conductivity σ increases to 10^6 S/m rapidly. We set the conductivity of aluminum as 3.56×10^7 S/m, and the permittivity of sapphire and GaAs as 10.5 and 13.1, respectively. A bare sapphire wafer identical to the sample substrate served as a reference. The transmission measured through the semiconductor metamaterial sample and the bare sapphire reference were exhibited in a time extent of the terahertz pulse.

The normalized amplitude transmission spectrum was measured under normal incidence with the E polarization along the y direction, and which can be defined as[31]

$$|t(w)| = \left| \frac{E_S(w)}{E_R(w)} \right|, \tag{1}$$

where $E_S(w)$ and $E_R(w)$[31] are Fourier transforms of the measured time-domain terahertz pulses of the sample and the reference substrate, respectively. We perpendicularly injected THz wave into our metamaterial surface at different frequencies (from 0.1 THz to 1 THz) and measured the transmission amplitude on the other side of our device.

As shown in Fig. 2(a), when the infrared light was turned off, the internal carriers in the semiconductor GaAs were in dynamic equilibrium. On the contrary, if the semiconductor GaAs was excited by the infrared laser pulse, the free carriers generated by the laser excitation were driven by the electric field on the semiconductor surface and accelerate. At the same time, the electrons and holes in the semiconductor were separated, so as to form a transient electric field in the semiconductor. The transient electric field destroyed the equilibrium state of the free carriers in the semiconductor, it led to plasma oscillation and sharp increase of conductivity. Therefore, through the irradiation of infrared light, the dynamic change of metamaterial structure could be realized, as shown in the illustrations of Fig. 2(a).

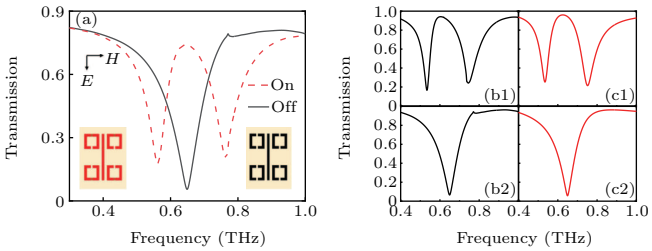


Fig. 2. (a) The transmission rate for two scenarios: with the infrared light switched on or off. Bottom right: infrared light off, with corresponding transmission amplitude marked by black line. Bottom left: infrared light on, with corresponding transmission amplitude marked by red dashed line. (b) Numerical simulation results for normalized spectra of the PIT metamaterial. (c) Theoretical fitting results.

Unlike previous methods of PIT manipulation (changing the material or the position of the unit) we were able to achieve the conversion between transparency and non-transmission simply by controlling the light source. When the light source illuminated the photosensitive semiconductor GaAs of the SRRs, we observed the PIT phenomenon in the optical transmission spectrum. When the central frequency was 0.65 THz, the transmittance suddenly rose rapidly from the minimum to form a transparent window. The PIT phenomenon was caused by the existence of two interference electric fields on the bright mode; the external electromagnetic field of the bright mode itself, and the electromagnetic field produced by the coupling with the dark mode. Therefore, the bright mode was not excited at 0.65 THz.

As illustrated in Fig. 2(a), the semiconductor GaAs in the gaps could be connected and conducted with the SRRs metal aluminum upon excitation by infrared light pulses, and exhibited high conductivity (in our simulation, the conductivity of GaAs was 1×10^6 S/m[32–34]). The transmission amplitude demonstrated a sharp transparency peak, with a transmission window around 0.65 THz. Without infrared light pulse illumination on the semiconductor, at this time, the conductivity of GaAs was 0 S/m and could not be connected or conducted with the SRRs metal aluminum and the metamaterial structure changed. The transmission amplitude had only one transmission trough at 0.65 THz. Therefore, we determined that our device was a controllable PIT device; and with the calculations, we determined that the modulation depth was greater than 87%. Near the bright mode resonance frequency, the SRR resonator displayed a resonance valley when the electric field E was along the x direction, but this did not appear when E was along the y direction. It was therefore clear that the four split-ring resonators were not directly coupled with the incident field E, which was used as the dark mode.

To explore the physical origin of the active PIT behavior, we adapted the widely used coupled Lorentz oscillator model to analyze the near-field interaction between the two elements

(metal and GaAs) in the PIT metamaterial unit cell. In PIT metamaterials, interference can be analytically described by the coupled Lorentz oscillator model (in order to simplify the coupling mode equation, this effect can be ignored and we do not introduce the coupling of two resonant rings on the same side in the derivation of the equation. The coupling effect between two resonant rings on the same side exists. However, as the distance between the two resonant rings is much farther than the value of parameter s, the coupling effect between the two resonant rings is too small compared to the coupling strength between CW and SRRs, and coupling strength between two resonant rings on the same side can be ignored), shown as

$$\begin{aligned} &\ddot{x}_1 + \gamma_1 \dot{x}_1 + \omega_1^2 x_1 + \kappa_{12} x_2 = gE, \\ &\ddot{x}_2 + \gamma_2 \dot{x}_2 + \omega_2^2 x_2 + \kappa_{21} x_1 = 0. \end{aligned} \tag{2}$$

The parameters x_1, x_2, γ_1, and γ_2 are the amplitudes and damping rates of the bright and dark modes, respectively. $\omega_1 = 2\pi \times 0.65$ THz and $\omega_2 = \omega_1 + \delta$ are the resonance frequencies of the bright and dark modes, respectively. The parameter κ_{12} is the coupling coefficient between the two modes and g is a geometric parameter indicating the coupling strength of the bright mode with the incident electromagnetic field E. According to Eq. (2), we can express the susceptibility χ of the PIT metamaterial unit cell by δ, κ_{12}, γ_1, and γ_2. The susceptibility χ_e of a PIT metamaterial layer with a thickness d is expressed as $\chi = \chi_e/d$.

Because our unit cell is much smaller than the resonant THz wavelength, we can consider the metamaterial layer to be an effective medium. The susceptibility χ_e of each unit can be expressed as

$$\chi_e = g \frac{-\omega^2 + i\gamma_2\omega + \omega_2^2}{(-\omega^2 + i\gamma_1\omega + \omega_1^2)(-\omega^2 + i\gamma_2\omega + \omega_2^2) - \kappa_{12}^2}. \tag{3}$$

As the metamaterial layer is much thinner than the wavelength of the terahertz wave, the far-field transmission of the PIT sample can be approximately related to the near field susceptibility as

$$|t| = \left| \frac{c(1+n_{sap})}{c(1+n_{sap}) - i\omega\chi_e} \right|, \tag{4}$$

where $c = 3 \times 10^8$ m/s is the light velocity in vacuum and $n_{sap} = 3.24$ is the refractive index of the sapphire.[25] Figures 2(b) and 2(c) show the analytical fit (using Eq. (4)) to the measured amplitude transmission spectra under different photo-excitation fluency, exhibiting very good congruence with simulation results.

Thus, it can be concluded from Figs. 2(b) and 2(c) that the active modulation of the PIT resonance arises from the change in the damping rate of the dark mode. Photo-excitation reduces loss in the SRRs and enhances the destructive interference between the bright and dark modes, which eventually leads to formation of the PIT resonance peak.

In the corresponding frequency domain spectrum, a PIT peak was observed, with a transmission amplitude of 85.8% at 0.65 THz. In order to demonstrate the magnetic amplitude of our device, we turned the infrared light on and off, as illustrated in Fig. 3. In Fig. 2(a), one can easily see that the magnetic energy is concentrated at the CW (bright mode). In contrast to the reaction when the infrared light was on, the semiconductor GaAs separated the SRRs when the light was off. Therefore, when one turns on the infrared light, the semiconductor carriers can be excited and the SRRs are the major point of interaction with the terahertz wave. In this scenario, one can acquire magnetic energy concentrated at the SRRs (dark mode) to achieve the transparency window.

Table 1. Parameters used for coupling between one bright mode and one dark mode.

Status	γ_1 (rad·ps^{-1})	γ_2 (rad·ps^{-1})	κ_{12} (rad^2·ps^{-2})	δ (rad·ps^{-1})
On	0.0800	0.2708	0.4119	0.0472
Off	0.078	0.2828	0.4181	0.0675

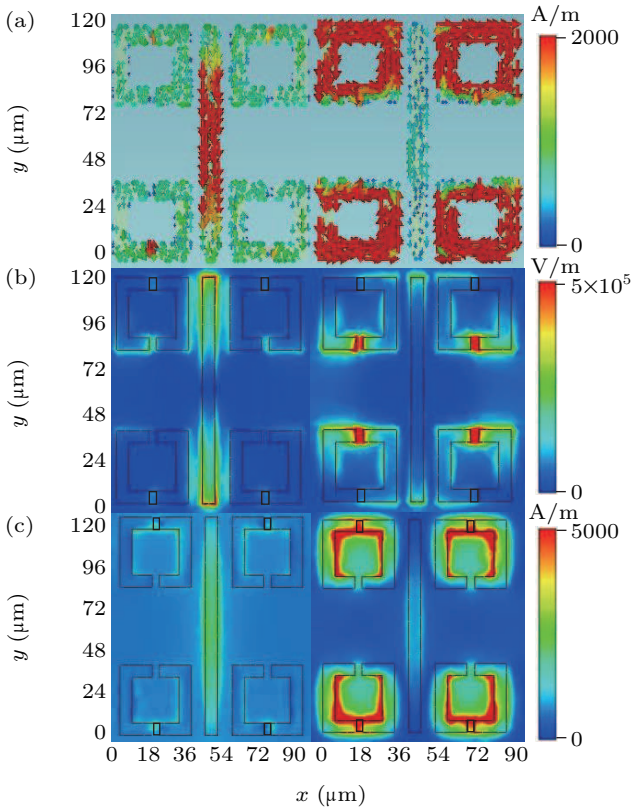


Fig. 3. (a) Surface current distributions at 0.65 THz. (b) Electric field distributions at 0.65 THz. (c) Magnetic field distributions at 0.65 THz. The right column shows the results with infrared light illumination.

In addition, in order to illustrate the physical mechanism of the PIT phenomenon, we applied field monitors in simulation to extract the electromagnetic resonance distribution at the enhanced transparency frequency. Figures 3(a)–3(c) demonstrate the distributions of surface current density, electric field,

and magnetic field at 0.65 THz, as shown in the left part of Fig. 3, without photo-excitation, the conductivity of GsAs was 0 S/m, the SRR gaps were disconnected; the CW and the hybrid SRRs exhibited the same resonant frequency, while the dark mode could not be excited. A Y-polarized incident wave excited the CW bar directly and led to an electric dipole resonance. No cross-coupling could be observed between the CW and the hybrid SRRs. On the contrary, as shown in the right part of Fig. 3, the conductivity of GaAs was 1×10^6 S/m and the free carriers could accelerate in GaAs gaps and aluminum SRRs, while the CW and hybrid SRRs exhibit the same frequency, and the dark mode can be excited. Y-polarized incidence excites the CW directly, and then the hybrid SRRs are strongly excited by the CW via near-field coupling. The external excitation from the incidence and the cross-coupling excitation from the hybrid SRR result in a cancellation effect for the electric dipole resonance on the CW. Thus, no current oscillation was observed on the CW, and the hybrid SRR exhibited a strong resonance.

We also studied the influence of SRR size on the peak value and bandwidth of resonance frequency caused by the PIT phenomenon. In order to understand the influence of coupling between the bright and dark modes on the PIT effect, we adjusted the structure of the unit cell and analyzed the influence of different parameters in the structure on the coupling results. First, we changed the distance s between the CW and the SRRs in the unit cell. By moving four SRRs symmetrically in the horizontal direction, we obtained the results shown in Fig. 4(a). It can be seen that when the distance s between the SRRs and the CW changes, the size of s is inversely proportional to the peak value of the transparent window. As the value of s increases, the peak value will decrease and the transmission rate will be lower. Because varying the size of s changes the value of the coupling strength, the larger the s decreases the coupling strength (see in Fig. 8(a)). Therefore, the energy transfer between the bright and dark modes starts to decrease, and the transparent window is becoming smaller, which shows the phenomenon in Fig. 4(a). The increasing of parameter d enlarges the resonant frequency and loss rate of SRRs, to lead the peak frequency of PIT shifting to high frequency and the width of the transparent window increasing (as shown in Fig. 4(b)). In the process of reducing the distance s, the peak value of the transparent window rose almost linearly and the bandwidth increased gradually. Obviously, the coupling between the bright and dark modes became stronger, however the Q (quality factor) is decreased. The Q factor can be calculated with the ratio of the resonance frequency to half peak width. when $s = 6$ μm, $Q = 4.5$. The results show that when the distance s decreases, so does the Q factor, whereas the coupling strength and radiation loss increase. In order to maximize the peak value of the transparent window and make the transmission rate the strongest, the distance between the SRRs and CW cannot be too large, as shown in Fig. 4(a).

We can regard the coupling mode between the bright mode and dark mode in the cell structure as an LC equivalent circuit. In an LC resonator, Q value is the key factor to measure the loss of components. The higher the Q value, the smaller the loss and the higher the efficiency. According to the relationship among the pass band, resonance frequency and quality factor Q, the larger the Q value is, the narrower the resonant pass band will be. If a wider pass band is needed, the smaller the Q value, the better.

Next, we discuss the different results when the length d of the gap in SRRs changes. Both the center frequency and the peak value in the transparent window are proportional to the size of d. The shorter the gap size, the larger the center frequency and the greater the peak value, as shown in Fig. 4(b). A shorter gap length will increase coupling.

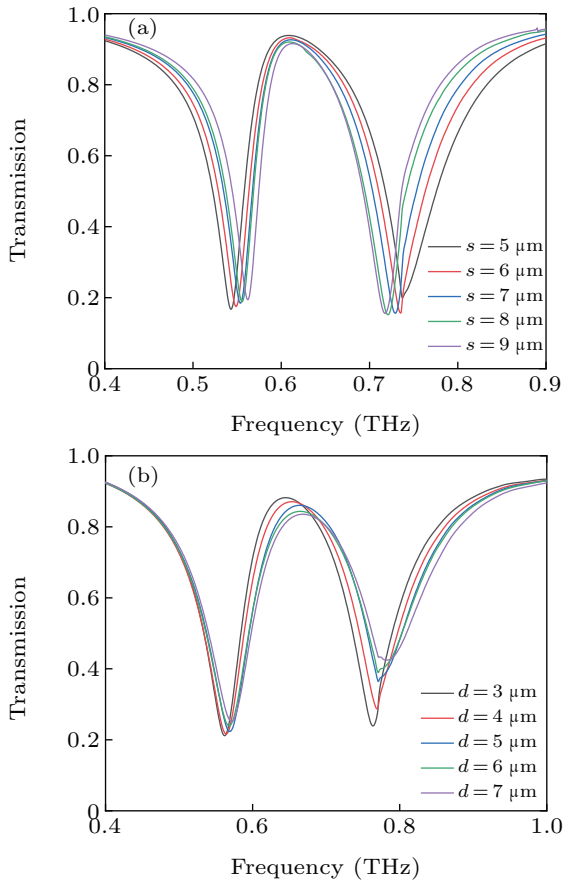


Fig. 4. (a) The frequency dependence of transmission with s as a parameter. (b) The frequency dependence of transmission with d as a parameter.

Thirdly, we take the cut wire as the center and rotate the SRRs in the cell structure to the left and right. During rotation, the four semiconductors are symmetrical with respect to the central perpendicular of the bright mode and the bright mode itself. The structure is shown in Fig. 5. When modulated, the PIT effect changes from the on to off state and from 0° to 60°, that is, the coupling between the bright and dark modes gradually disappears. This is because the dark mode is symmetri-

cal with respect to the y polarization direction of the incident electromagnetic wave at 0° and hardly excited at 0.65 THz. Through the passive coupling of the bright mode, the PIT effect is formed by interference with the bright mode field. In the process of rotation to 180°, the symmetry of the dark mode relative to the polarization direction is broken, which means that it can be directly excited by the incident field; thus the destructive interference between the bright and dark modes is weakened, so the transparent window disappears gradually, and almost disappears at about 260°. Between 60° and 260°, there is no transparent window. Between 260° and 360°, the transparent window gradually appears. Rotation of SRRs changes the coupling strength between bright and dark modes, which mainly affects the PIT spectrum. We employ the couple mode equation to fit the SRRs curves with different rotation angles and the corresponding coupling strength. To give few examples to demonstrate, when rotation angles are $\theta = 0°$, $\theta = 20°$, $\theta = 60°$, $\theta = 260°$, and $\theta = 300°$, respectively, we obtain the corresponding coupling strengths $\kappa = 0.4119$ rad^2·ps^{-2}, $\kappa = 0.3245$ rad^2·ps^{-2}, $\kappa = 0.1067$ rad^2·ps^{-2}, $\kappa = 0.1153$ rad^2·ps^{-2}, $\kappa = 0.3431$ rad^2·ps^{-2}. To sum up, when the rotation angle is between 0°–180°, the coupling strength decreases with the increasing of the angle; when the rotation angle is between 180°–360°, the coupling strength starts to increase with the gradual increase of the angle. As we can see that when the coupling strength is between 60° and 260°, the coupling between the bright mode and the dark mode is relatively small which causes the PIT phenomenon to disappear.

Finally, we studied the effect of photosensitive semiconductor GaAs on the PIT phenomenon in terms of changing the conductivity. As shown in Fig. 5(f), when the conductivity of GaAs was 0 S/m, the semiconductors did not conduct to the SRRs. After the excitation of the infrared light field, GaAs becomes the metalloid properties, which causes the original SRRs with varying the geometrical structure from two gaps to one gap. Thus, the resonance frequency moves to the low frequency. When the conductivity of GaAs changes to 1×10^5 S/m, the TM resonant frequency corresponding to the dark mode is 0.635 THz. When the conductivity of GaAs is 0 S/m and 1×10^4 S/m, the TM resonance peak does not appear in 0 THz–2 THz. The TM resonance frequency of the dark mode is close to that of the TE resonance frequency of the bright mode, so the PIT phenomenon will occur. When the conductivity reached 1×10^6 S/m, the window value reached its maximum and the transmission reached 0.738. In the same way, the length of the CW will have a certain impact on the results. When the length of the CW increase, the resonance frequency will decrease, and the coupling strength will become weak, which we will not discuss here.

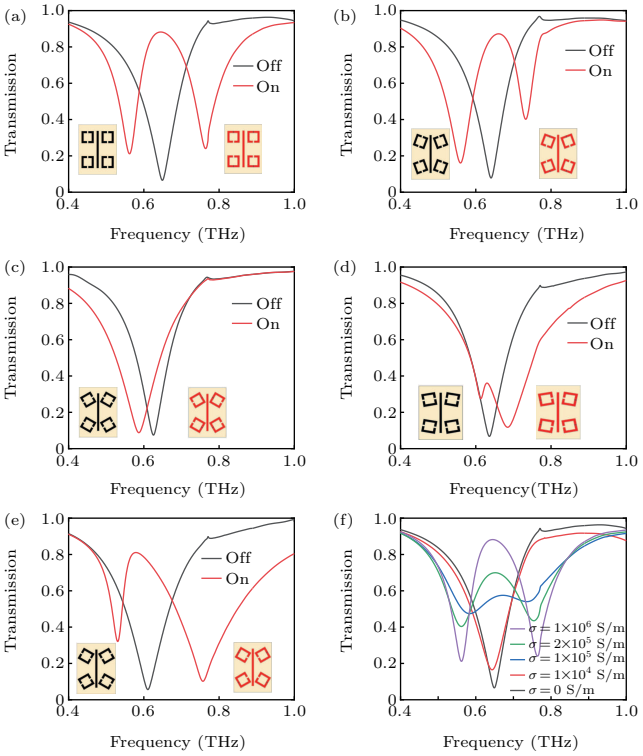


Fig. 5. Transmission results and structures of the unit cell after rotating the SRRs. (a) $\theta = 0°$, (b) $\theta = 20°$, (c) $\theta = 60°$, (d) $\theta = 20°$, (e) $\theta = 300°$, (f) the frequency dependence of transmission with GaAs conductivity δ as a parameter.

4. Multiple dark modes

In the previous section, we discussed active control of the metamaterial structure to produce the PIT effect, analyzing coupling between one bright mode and one dark mode. Now, we will further discuss couplings between one bright mode and several dark modes. Due to the coupling between the bright and dark modes, the energy is completely transferred from the bright mode to the dark mode, leading to a sharp transparency window in the otherwise broad absorption spectrum. In this section, we take the case of one bright mode and two dark modes as an example.

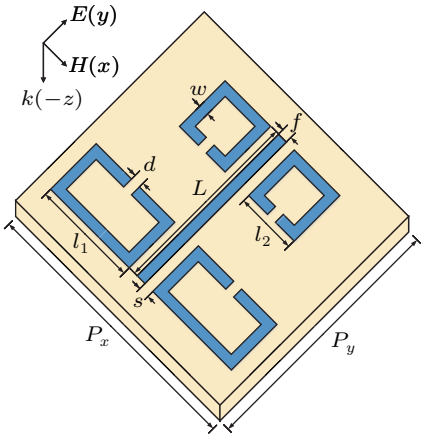


Fig. 6. The unit cell of a metamaterial with one bright mode and two dark modes. The geometrical parameters are: $L = 90$ μm, $l_1 = 50$ μm, $l_2 = 29$ μm, $w = 5$ μm, $s = 6$ μm, $d = 3$ μm, $f = 5$ μm, $P_x = 130$ μm and $P_y = 120$ μm.

The unit cell of the proposed plasmon-induced transparency metamaterial is shown in Fig. 6. The symmetrical structure consists of an aluminum cut wire (CW) and two pairs of aluminum split-ring resonators (SRRs) of different sizes. In this structure, the CW resonator (bright mode) could be excited by the incident field, and the two pairs of SRRs with different sizes were considered to be the dark modes. The metallic resonators were also made from 200-nm-thick aluminum, fabricated in a square lattice on a 0.64-mm-thick sapphire substrate.

In this section, the interference in the plasmon-induced transparency metamaterials can be analytically described by the coupled Lorentz oscillator model, the expressions are shown as follows:[35]

$$\begin{aligned}
&\ddot{x}_1 + \gamma_1\dot{x}_1 + \omega_1^2 x_1 + \kappa_1 x_2 + \kappa_2 x_3 = gE,\\
&\ddot{x}_2 + \gamma_2\dot{x}_2 + \omega_2^2 x_2 + \kappa_1 x_1 = 0,\\
&\ddot{x}_3 + \gamma_3\dot{x}_3 + \omega_3^2 x_3 + \kappa_2 x_1 = 0,
\end{aligned} \tag{5}$$

where the parameters x_1, x_2, x_3, γ_1, γ_2, and γ_3 are the amplitudes and damping rates of the bright and dark modes, respectively. The parameters κ_1 and κ_2 are the coupling coefficients between the bright mode and the first and second dark modes, respectively. The parameter g is a geometric parameter indicating the coupling strength of the bright mode with the incident electromagnetic field E. The amplitudes of the three modes of each unit can be expressed as

$$\begin{aligned}
x_1 &= gE\frac{(-\omega^2+\mathrm{i}\gamma_2\omega+\omega_2^2)(-\omega^2+\mathrm{i}\gamma_3\omega+\omega_3^2)}{(-\omega^2+\mathrm{i}\gamma_1\omega+\omega_1^2)(-\omega^2+\mathrm{i}\gamma_2\omega+\omega_2^2)(-\omega^2+\mathrm{i}\gamma_3\omega+\omega_3^2)-\kappa_1^2(-\omega^2+\mathrm{i}\gamma_3\omega+\omega_3^2)-\kappa_2^2(-\omega^2+\mathrm{i}\gamma_2\omega+\omega_2^2)},\\
x_2 &= gE\frac{\kappa_2(-\omega^2+\mathrm{i}\gamma_2\omega+\omega_2^2)}{(-\omega^2+\mathrm{i}\gamma_1\omega+\omega_1^2)(-\omega^2+\mathrm{i}\gamma_2\omega+\omega_2^2)(-\omega^2+\mathrm{i}\gamma_3\omega+\omega_3^2)-\kappa_1^2(-\omega^2+\mathrm{i}\gamma_3\omega+\omega_3^2)-\kappa_2^2(-\omega^2+\mathrm{i}\gamma_2\omega+\omega_2^2)},\\
x_3 &= gE\frac{\kappa_1(-\omega^2+\mathrm{i}\gamma_3\omega+\omega_3^2)}{(-\omega^2+\mathrm{i}\gamma_1\omega+\omega_1^2)(-\omega^2+\mathrm{i}\gamma_2\omega+\omega_2^2)(-\omega^2+\mathrm{i}\gamma_3\omega+\omega_3^2)-\kappa_1^2(-\omega^2+\mathrm{i}\gamma_3\omega+\omega_3^2)-\kappa_2^2(-\omega^2+\mathrm{i}\gamma_2\omega+\omega_2^2)}.
\end{aligned} \tag{6}$$

Hence, the effective electric susceptibility of the metamaterial can be written as

$$\chi_e \approx k\frac{(-\omega^2+\mathrm{i}\gamma_2\omega+\omega_2^2)(-\omega^2+\mathrm{i}\gamma_3\omega+\omega_3^2)}{(-\omega^2+\mathrm{i}\gamma_1\omega+\omega_1^2)(-\omega^2+\mathrm{i}\gamma_2\omega+\omega_2^2)(-\omega^2+\mathrm{i}\gamma_3\omega+\omega_3^2)-\kappa_1^2(-\omega^2+\mathrm{i}\gamma_3\omega+\omega_3^2)-\kappa_2^2(-\omega^2+\mathrm{i}\gamma_2\omega+\omega_2^2)}. \tag{7}$$

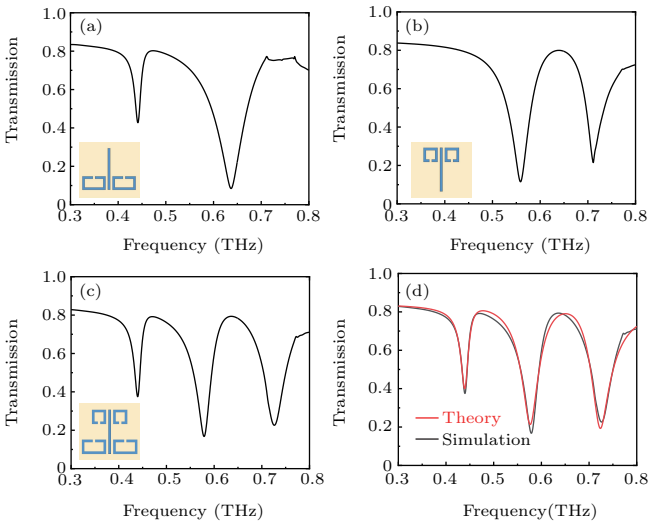


Fig. 7. (a) The transmission spectrum for coupling between the bright mode and the first dark mode. (b) The transmission spectrum for coupling between the bright mode and the second dark mode. (c) Spectral line of the designed structure. (d) The black line shows the simulation results while the red line shows the theoretical fitting results.

Substituting Eq. (7) into Eq. (5), the expression of the transmission spectrum can be obtained. For parameters in the coupled mode equation, such as resonant frequency and loss rate, we can obtain them by simulating the bright mode or dark mode separately. For the bright mode, we use CST Microwave Studio^{TM} to get the transmission spectrum of CW, where the frequency corresponding to the peak is the resonant frequency ω_1, the half-height full-width is the loss rate γ_1. For the dark mode, we set the polarization direction of the terahertz wave as X direction to obtain transmission lines and the dark mode parameters ω_2, ω_3, γ_2, and γ_3. Then, the parameters ω_1, ω_2, ω_3, γ_1, γ_2, and γ_3 are substituted into the coupling mode equation, and the coupling strength κ can be obtained by fitting the simulated curve.[36] Figure 7(c) shows the results of fitting analysis for the simulated spectral lines.

To elucidate the coupling mechanism between one bright mode and two dark modes, the couplings between the bright mode and the dark modes were visualized in Fig. 7. The PIT effect was obtained via coupling between the bright mode and the first dark mode at 0.454 THz, which we considered the result of strong coupling between the bright mode and the second dark mode at 0.649 THz. Therefore, the transmission spectrum in Fig. 7(c) was superimposed with the spectrums in Figs. 7(a) and 7(b). We employ CST Microwave Studio^{TM} to get the transmission spectrum of their separate structures for coupling between the bright and two dark modes. From the simulation results, the frequency of the bright mode, the first dark mode and the second dark mode are corresponding 0.6035 THz, 0.454 THz, and 0.649 THz respectively. Since the CW was coupled with incident field E, the incident energy was absorbed by the bright mode, which allowed the

energy of the bright mode to transfer into the dark modes via coupling. Due to the coupling between the bright mode and two dark modes, two PIT peaks appear when the two dark modes absorb the energy of bright mode at 0.454 THz and 0.649 THz, respectively, resulting in the spectral lines shown in Fig. 7(c). The phenomenon of coupling between one bright mode and multiple dark modes could be seen as the result of linear superposition of the coupling between the bright mode and each dark mode. The linear superposition of spectral lines indicated linear superposition of energy. The energy contained in the bright mode would be distributed into the two dark modes. The coupling strengths obtained by fitting are $\kappa_1 = 0.1938\ \mathrm{rad^2{\cdot}ps^{-2}}$ and $\kappa_2 = 0.3148\ \mathrm{rad^2{\cdot}ps^{-2}}$ (see Fig. 8(b)).

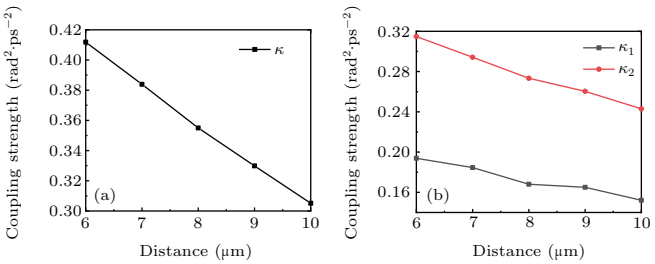


Fig. 8. The variations of the fitting coupling strength with respect to distance parameter *s*, when the transmission spectrum line is fitted. (a) Coupling between bright mode and one dark mode, (b) coupling between bright mode and two dark modes.

Compared with the smaller SRR, coupling strength between the bright mode and the first dark mode was smaller. The frequency of the transparent window's peak value would shift to the left since the CW would have some energy, as shown in Fig. 7(a). In addition, the effective distance between the bright mode and the first dark mode was larger than that between the bright mode and the second dark mode; thus the coupling strength was smaller, which was consistent with the size of the coupling strength obtained by fitting. We also prove this by changing the distance parameter *s* between the bright and dark modes in Fig. 8. We can see that the coupling strength decreases with the increase of distance *s* in terms of the overall trend.

To further prove that the spectral lines are formed by linear superposition, figures 9(a) and 9(b) show the two-dimensional electric field and surface current distribution of the cell at the focused transparent window. The energy of the CW mostly transfers into the larger SRR or the smaller SRR, as shown in Figs. 9(a) and 9(b). At 0.4704 THz, CW is excited (but not wholly excited) by the external terahertz excitation source, and due to the coupling with the dark mode 1, it can cause the resonance of the dark mode 1, but since the dark mode appears TM resonance at 0.4704 THz, most of the energy could be distributed at the gap of the dark mode 1. At 0.6357 THz, CW is excited under the external terahertz excitation source, resulting in dipole resonance, and the coupling with the dark mode causes the resonance of the dark mode. Hence, both dark modes have energy distribution. However, the TM resonance of dark mode 2 occurs at 0.6357 THz, so most of the energy can be distributed at the gap of dark mode 2.

Table 2. Parameters used for coupling between one bright mode and two dark modes.

Status	ω_1 (rad·ps^{-1})	ω_2 (rad·ps^{-1})	ω_3 (rad·ps^{-1})	γ_1 (rad·ps^{-1})	γ_2 (rad·ps^{-1})	γ_1 (rad·ps^{-1})
Fitting value	$2\pi \times 0.6035$	$2\pi \times 0.4535$	$2\pi \times 0.6488$	0.1	0.192	0.2119

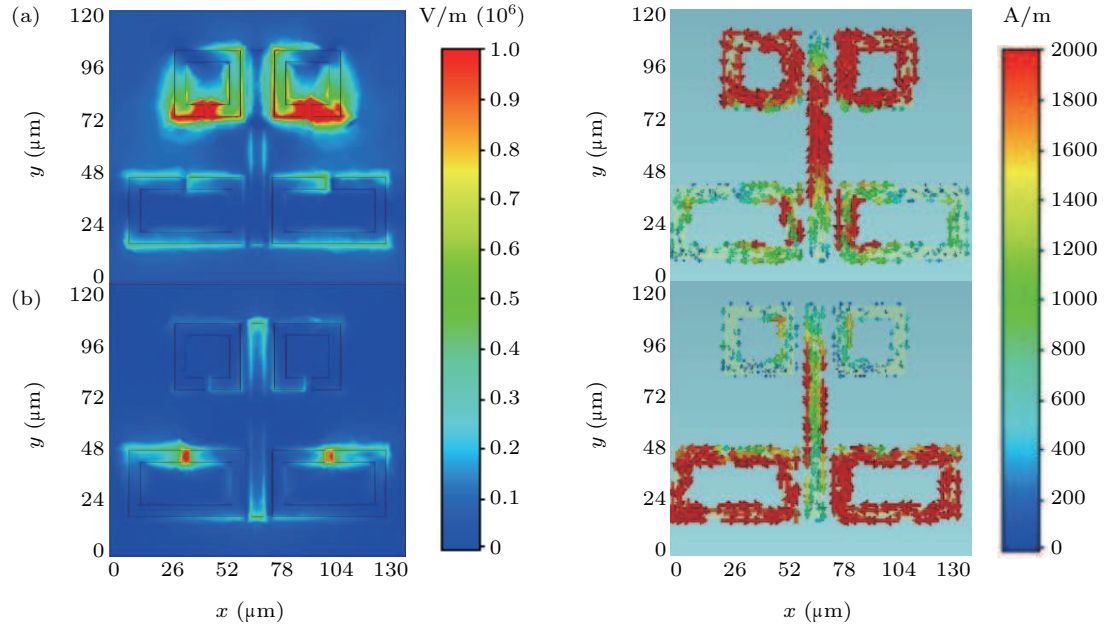


Fig. 9. Electric field and surface current distributions at 0.6357 THz (a), and 0.4704 THz (b).

5. Conclusion

In this study, we realized a photo-controlled PIT metamaterial in the THz regime. By inserting a photosensitive semiconductor GaAs into the SRR gaps, the on-to-off state of the PIT resonance can be actively controlled under different levels of excitation from optical pulses. The controllable PIT can be achieved by utilizing active control. We found that controllable switching the PIT (transparency window) on or off was possible via exciting carriers of semiconductors with different intensities external infrared light at a frequency of 0.65 THz; this allowed us to simultaneously obtain impressive modulation depth ($> 87\%$). We investigated the transmission property of the PIT sample under different optical intensity excitation and the influences of different structural sizes on the PIT phenomenon. Finally, couplings between one bright mode (CW) and several dark modes (SRRs) of different sizes were discussed. The interference analytically described by the coupled Lorentz oscillator model elucidated the coupling mechanism and it can be considered the result of linear superposition of the coupling between the bright mode and each dark mode. The proposed metamaterials structure are promising for application in the fields of THz communications, optical storage, optical display, and imaging.

Acknowledgments

Project supported by the National Science and Technology Major Project (Grant No. 2017ZX02101007-003), the National Natural Science Foundation of China (Grant No. 61965005), the Natural Science Foundation of Guangxi Province (Grant No. 2019GXNSFDA185010), Guangxi Distinguished Expert Project, Foundation of Guangxi Key Laboratory of Optoelectronic Information Processing (Grant No. GD20104), the National Natural Science Foundation of China (Grant No. 62105187), the Natural Science Foundation of Shandong Province, China (Grant No. ZR2021QF010), and the Innovation Project of Guang Xi Graduate Education (Grant No. YCSW2020158).

References

[1] Marangos J P 1998 *Journal of Modern Optics* **45** 471
[2] Siegel P H 2002 *IEEE Transactions on microwave theory and techniques* **50** 910
[3] Siegel P H 2004 *IEEE Transactions on Microwave Theory and Techniques* **52** 2438
[4] Kawase K, Shikata J and Ito H 2002 *J. Phys. D: Appl. Phys.* **35** R1
[5] Manjappa M and Singh R 2020 *Adv. Opt. Mater.* **8** 1901984
[6] Huang W, Qu X W and Yin S 2020 *IEEE Journal of Selected Topics in Quantum Electronics* **27** 8400107
[7] Huang W, Liang S J and Kyoseva E 2018 *Carbon* **127** 187
[8] Huang W, Yin S and Zhang W 2019 *New J. Phys.* **21** 113004
[9] Peng J, He X and Shi C 2020 *Physica E* **124** 114309
[10] He X Y, Liu F and Lin F T 2021 *J. Phys. D: Appl. Phys.* **54** 235103
[11] Li J S and Chen X S 2020 *Chin. Phys. B* **29** 078703
[12] Dimova E, Huang W and Popkirov G 2016 *Opt. Commun.* **366** 382
[13] Huang W, Hao X Y and Cheng Y 2021 *J. Lightwave Technol.* **39** 7925
[14] Chen X Y, Tian Z and Li Q 2020 *Chin. Phys. B* **29** 077803
[15] Wu C H, Khanikaev A B and Shvets G 2011 *Phys. Rev. Lett.* **106** 107403
[16] Luk'yanchuk B, Zheludev N I and Maier S A 2010 *Nat. Mater.* **9** 707
[17] Zhang L, Tassin P and Koschny T 2010 *Appl. Phys. Lett.* **97** 241904
[18] Zhang J J, Xiao S S and Jeppesen C 2010 *Opt. Express* **18** 17187
[19] Yin S, Hu F R and Chen X Y 2019 *J. Opt.* **21** 025101
[20] Wu J Y, Xu X F and Wei L F 2020 *Chin. Phys. B* **29** 094202
[21] Yin S, Lu X C and Xu N N 2015 *Scientific Reports* **5** 16440
[22] Guo L, Ma J and Chen S 2018 *Plasmonics* **13** 1941
[23] Liu X J, Gu J Q and Singh R 2012 *Appl. Phys. Lett.* **100** 131101
[24] Li Z Y, Ma Y F and Huang R 2011 *Opt. Express* **19** 8912
[25] Gu J, Singh R and Liu X 2012 *Nat. Commun.* **3** 1151
[26] Bai Q, Liu C and Chen J 2010 *J. Appl. Phys.* **107** 093104
[27] Thuy V T T, Tung N T and Park J W 2010 *J. Opt.* **12** 115102
[28] Fan Z F, Tian Z Y and Wan W J 2017 *Acta Phys. Sin.* **66** 087801 (in Chinese)
[29] Li G S, Yan F P and Wang W 2019 *Chin. J. Lasers* **46** 0114002
[30] Meng Q L, Zhang Y and Zhong Z Q 2018 *J. Modern Opt.* **65** 2086
[31] Azad A K, Dai J M and Zhang W L 2006 *Opt. Lett.* **31** 634
[32] Chen X Y, Ghosh S and Xu Q 2018 *Appl. Phys. Lett.* **113** 061111
[33] Shen X and Cui T J 2012 *J. Opt.* **14** 11
[34] Wang G C, Zhang J N and Zhang B 2016 *Opt. Commun.* **374** 64
[35] Liu J X, Jin K L and He X Y 2019 *Appl. Phys. Express* **12** 075010
[36] Huang W, Liu S Y and Cheng Y 2021 *New J. Phys.* **23** 093017